THE JOURNAL OF PHYSICAL CHEMISTRY C

Article

pubs.acs.org/JPCC

# Tuning the Electronic and Magnetic Properties of Phosphorene by Vacancies and Adatoms

Pooja Srivastava, K. P. S. S. Hembram, Hiroshi Mizuseki, Kwang-Ryeol Lee, Sang Soo Han,* and Seungchul Kim*

Computational Science Research Center, Korea Institute of Science and Technology (KIST), Hwarangno 14-gil 5, Seongbuk-gu, Seoul 136-791, Republic of Korea

Supporting Information

**ABSTRACT:** We report a density functional theory (DFT) study regarding the effects of atomic defects, such as vacancies and adatom adsorption, on the electronic and magnetic properties of phosphorene (a two-dimensional monolayer of black phosphorus). A monovacancy in the phosphorene creates an in-gap state in the band gap of pristine phosphorene and induces a magnetic moment, even though pristine phosphorene is nonmagnetic. In contrast, both planar and staggered divacancies do not change the magnetic properties of phosphorene, although a staggered divacancy creates states in the gap. Our DFT calculations also show that adsorption of nonmetallic elements (C, N, and O) and transition metal elements (Fe, Co, and Ni) can change the magnetic properties of phosphorene with or without vacancies. For example, the nonmagnetic pristine phosphorene becomes magnetic after the adsorption of N, Fe, or Co adatoms, and the magnetic phosphorene with a monovacancy becomes nonmagnetic after the adsorption of C, N, or Co atoms. We also demonstrate that for O- or Fe-adsorbed monovacancy structure the electronic and magnetic properties are tunable via the control of charge on the phosphorene system. These results provide insight for achieving metal-free magnetism and a tunable band gap for various electronic and spintronic devices based on phosphorene.

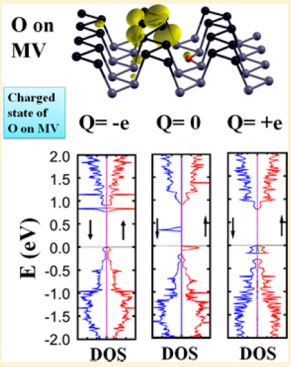


## INTRODUCTION

In the search for novel two-dimensional (2D) materials, phosphorene has been synthesized by mechanical exfoliation and nanodevices, such as p−n junction and field effect transistors, have been successfully fabricated.[1−5] Theoretical efforts have also been made to investigate single- and few-layered phosphorene sheets[1,6−11] and nanoribbons.[12−14] A heterojunction of $MoS_2$ and phosphorene can lead to an efficient solar cell with power conversion efficiency ∼18%.[17] Strained phosphorene can be an efficient photocatalyst for visible light water splitting.[18] Also, several studies reported that black phosphorus can be a potential candidate for an anode material of Li-/Na-ion is also quite impressive.[19,20]

Other 2D materials, such as graphene, *h*-BN, and $MoS_2$, have been widely studied in various contexts. Graphene is the only material that is made up of a single element and remains flat, while *h*-BN contains two different elements and also remains flat. Although $MoS_2$ forms a monolayer, the geometrical arrangements of Mo and S do not lie in the same layer. In this regard, phosphorene is a new platform that consists of a single element and does not remain flat. Instead, the phosphorus atoms are evenly distributed between two half layers, forming a corrugated monolayer, which leads to different properties compared with graphene, *h*-BN, $MoS_2$, etc.

The electronic band gap of phosphorene has been investigated using several density functional theory (DFT) calculations. According to those calculations, phosphorene is a semiconductor with electronic band gaps in the range of 0.90 eV (PBE level) to 1.53 eV (hybrid functional level).[1,8] Its band gap decreases, going from a monolayer to a few layers with power law[1,7,8] $\sim N^{\alpha}$, where $N$ is the number of layers and $0 < \alpha < 2$. In addition, a GW calculation predicts the quasiparticle band gap of 2.0 eV for phosphorene.[7] Electron transport measurements show that the field-effect mobility range is 205−1000 $cm^2/(V\ s)$,[1,3,5] and the on/off ratio ranges from $10^4$ to $10^5$.[1−5] We infer that the wide variation in the above values might be due to differences in the layer thickness, which ranges from 3 layers to 60 layers, and different external conditions (e.g., temperature, pressure, and contact material). Moreover, according to the Hall measurement,[1] phosphorene has an anisotropic transport nature, and the electron mobility differs in the two in-plane orthogonal directions. Liu et al.[1] attributed the anisotropic current flow to the ridged structure of phosphorene. Fei et al.[9] showed that the anisotropy is due to the different effective masses in the two directions, which can be tailored by the application of strain. Peng et al.[12] reported that with compressive or tensile strain on phosphorene along an armchair or zigzag direction the band gap can undergo a direct−indirect transition.

As with other as-synthesized materials, phosphorene contains defects such as vacancies, and these defects can affect the properties of the material significantly. Zhang et al.[21] directly

**Received:** November 5, 2014
**Revised:** March 6, 2015
**Published:** March 9, 2015





DOI: 10.1021/jp5110938
J. Phys. Chem. C 2015, 119, 6530−6538

observed vacancies on few-layered phosphorene with scanning tunneling microscopy (STM). The defect-induced states can also act as scattering centers[22,23] and can affect the transport properties of phosphorene. In an atomic force microscopy (AFM) study performed under ambient conditions, few-layered phosphorene was found to be seriously degraded after 1 h of exfoliation.[3,24] To prevent such degradation, a low oxygen and low humidity environment is suggested.[3,25] Although black phosphorus is itself very stable,[26] phosphorene shows a variety of activity within such an environment, an area of research that is open to be explored. Therefore, an electronic structure study of defective phosphorene is desirable for understanding the fundamental properties of phosphorene and promoting its successful application in electronic devices.

In the present work, we use first-principles calculations systematically to investigate the effects of vacancies and adsorption of various nonmetallic and transition metal (TM) elements on the electronic and magnetic properties of pristine and defective phosphorene. We find that the vacancies and adatoms can change the electronic and magnetic properties of phosphorene significantly. Indeed, we find that a magnetic moment of adatom-adsorbed phosphorene can be tuned by controlling the Fermi level, which can be achieved by applying an electric field vertically or by choosing the appropriate substrate.

## COMPUTATIONAL DETAILS

To investigate the electronic structure and magnetic properties of phosphorene, we performed *ab initio* density functional theory (DFT) calculations implemented in the Vienna *ab initio* simulation package (VASP)[27,28] within the generalized gradient approximation proposed by Perdew, Burke, and Ernzerhof (PBE).[29] The electronic wave functions were expanded in a plane-wave basis set using a kinetic energy cutoff of 500 eV. The effects of the core electrons and nuclei were replaced by projector augmented wave (PAW) potentials.[30] To include the effect of van der Waals interactions, we adopt Grimme's DFT-D2 approach[31] implemented in the VASP software. Additionally, to examine the stability of the phosphorene with a vacancy, we performed a Born–Oppenheimer *ab initio* molecular dynamics (ABMD) simulation at 300 K, where the temperature was adjusted via a Nosé thermostat[32−34] with an MD time step of 1 fs. The ABMD was carried out with the VASP software.

Phosphorene was represented by a repeated-layer geometry. We examine the convergence of calculated values as well as a finite size effect using 4 × 3 (48 P atoms), 6 × 4 (96 P atoms), and 8 × 6 supercells (192 P atoms) and considered one defect in the supercell, which corresponds to defect concentrations of 2.0%, 1.0%, and 0.5%, respectively. Three supercells are presented in the Supporting Information (Figure S1). Adsorption energies are converged with less than 0.1 eV of error at a middle-sized 6 × 4 supercell as well as magnetic moments. Thus, defects and adatoms at the 6 × 4 supercell are well separated and can be considered isolated defects. To avoid any interaction between successive layers, the layers were separated by an 18 Å vacuum. For structure optimization, reciprocal space sampling was performed with a 3 × 3 × 1 Monkhorst–Pack[35] *k*-point mesh for a 4 × 3 × 1 supercell and was equally dense for other sized supercells. We considered the structure to be converged when all of the force components were smaller than 0.01 eV/Å. Our PBE calculation for pristine phosphorene yields lattice parameters along the armchair ($x$) and zigzag ($y$) directions of $a$ = 3.31 Å and $b$ = 4.57 Å, respectively, which are similar to the previous theoretical studies.[1,8,10] In addition, our PBE calculation including van der Waals interactions for black phosphorus (BP) shows lattice parameters of $a$ = 3.32 Å, $b$ = 4.44 Å, and $c$ = 10.49 Å, which are close to the experimental observations.[5,36,37]

According to our band structure calculation for pristine phosphorene (Figure 1e), both the valence band maximum (VBM) and conduction band minimum (CBM) are located at the Γ point of the reciprocal space and are separated by a gap of 0.88 eV, revealing a direct semiconducting band gap in the system. The VBM is due to the $3p_z$ states, and CBM is the mixture of the $3p_y$, $3p_z$, and 3s states. The electronic bands are more dispersive along the Γ to Y (armchair) direction than the Γ to X (zigzag) direction. This directionally dispersive nature leads to anisotropic electrical conductance, which has been observed experimentally.[1−5]

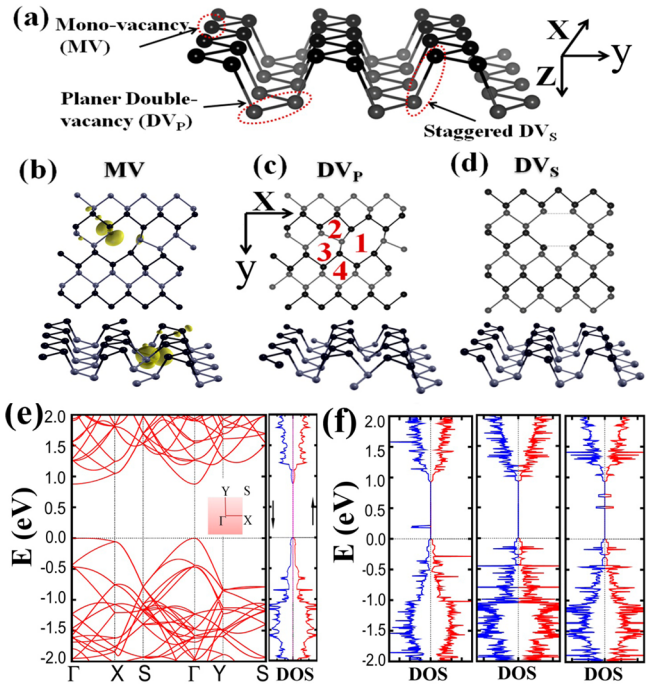


**Figure 1.** Optimized structures of (a) pristine, (b) MV−, (c) $DV_P$−, and (d) $DV_S$−phosphorene. (e) Electronic band structures and DOS of pristine phosphorene and (f) DOS of MV, $DV_P$, and $DV_S$ from left to right. P atoms in the upper and lower half layer are represented by black and gray balls for clarity. Spin density plot for MV−phosphorene is shown in (b).

To confirm the reliability of our PBE calculations, we also considered the Heyd–Scuseria–Ernzerhof (HSE06)[38] hybrid exchange correlation (XC)-functional. The HSE06 calculation for pristine phosphorene leads to lattice parameters of $a$ = 3.29 Å and $b$ = 4.54 Å, which are similar to the PBE calculation ($a$ = 3.31 Å and $b$ = 4.57 Å). Our HSE06 calculation provides a direct band gap of 0.30 eV for the black phosphorus, which is in excellent agreement with the previous HSE06 result[39] and the experimental value of ∼0.30 eV.[40,41] For pristine phosphorene, our HSE06 calculation shows a band gap of 1.5 eV, which is similar to previous studies.[1,39] We find that electronic dispersions within both HSE06 and PBE are similar, although the PBE functional leads to a lower band gap (0.88 eV) than that of the HSE06 functional. As already mentioned, because the PBE and HSE06 calculations for pristine phosphorene


DOI: 10.1021/jp5110938
J. Phys. Chem. C 2015, 119, 6530−6538

Table 1. Adsorption Energy ($E_{ads}$), Formation Energy ($\Delta E$), and Magnetic Moment of Adatom-Absorbed Pristine/MV/DV−Phosphorene[a]

| | $E_{ads}$ (eV) | | | $\Delta E$ (eV) | | | mag moment ($\mu_B$) | | |
|---|---|---|---|---|---|---|---|---|---|
| adatom | pristine | MV | DV | pristine | MV | DV | pristine | MV | DV |
| C | −4.82 | −7.92 | −5.29 | 3.14 | 0.04 | 2.67 | 0.0 (0.0) | 1.0 (1.0) | 0.0 |
| N | −3.30 | −6.28 | −4.96 | 1.89 | −1.09 | 0.23 | 1.0 (1.0) | 0.0 | 1.0 |
| O | −5.32 | −5.83 | −5.80 | −1.92 | −2.44 | −2.42 | 0.0 (0.0) | 1.0 (1.0) | 0.0 |
| Fe | −3.82 | −5.76 | −5.38 | 1.47 | −0.45 | −0.07 | 2.0 | 1.0 | 2.0 |
| Co | −4.45 | −6.48 | −5.34 | 0.92 | −0.88 | 0.26 | 1.0 | 0.0 | 1.0 |
| Ni | −4.51 | −5.86 | −5.30 | 0.36 | −0.99 | −0.43 | 0.0 | 1.0 | 0.0 |

[a]Magnetic moment from the calculations with the HSE06 XC-functional are given in parentheses. All values were calculated with an 8 × 6 supercell but with a 4 × 3 supercell for HSE06 calculations. $E_{ads} = E_{ph+X} - (E_{ph} + E_X^{atm})$, $\Delta E = E_{ph+X} - (E_{ph} + E_X)$, where each term is the energy of adatom-adsorbed phosphorene ($E_{ph+X}$), pristine or defective phosphorene ($E_{ph}$), and element $X$ in atomic ($E_X^{atm}$) and bulk or gas molecule ($E_X$) states.

predict similar atomic structures and lattice parameters, the HSE06 calculations based on geometries optimized with the HSE06 (self-consistent HSE06; sc-HSE) and PBE methods (1-shot HSE) provide similar total energies (only ∼5 meV/atom) and electronic structure (e.g., band gap difference of only 0.02 eV). We also confirmed that both of the sc-HSE06 and PBE provide similar internal structure and magnetic moment of the phosphorene with monovacancy (Figure S8). Because of high computational demand of sc-HSE calculations, we did not perform the sc-HSE calculation for all the phosphorene systems considered in this study. Therefore, 1-shot HSE (henceforth HSE) calculations are done to verify the electronic and magnetic properties of pristine and defective phosphorene (with/without nonmetallic adatom), and we found that these are qualitatively same at both the PBE and HSE levels.

For transition metal elements, the electron correlation effect is very important due to the localized d-orbital. Thus, we additionally considered the DFT+$U$ method for the TM-adsorbed phosphorene systems, where the Hubbard parameter $U$ is added at the GGA level. We used the rotationally invariant DFT+$U$ formalism proposed by Dudarev et al.,[42] where $U_{eff} = U - J$ was used instead of individual $U$ and $J$ values. One can calculate $U$ and $J$ by treating these as empirical parameters and fitting them to experimental values.[43,44] However, as no experimental value of $U$ or exchange parameter $J$ is available for TM adatom-adsorbed phosphorene, we considered different values of $U_{eff}$ ranging from weak to intermediate coupling regime ($U_{eff}$ = 2, 4, and 6 eV) to understand the effect of $U$. The properties of TM-adsorbed phosphorene may be quite sensitive to the value of $U_{eff}$;[44] therefore, our results should be taken as a qualitative indication rather than a quantitative indication of the correlation effect. Consideration of the HSE method can provide accurate results for the TM-adsorbed phosphorene systems. However, the PBE+$U$ calculation is less time-consuming than the HSE calculation, and PBE+$U$ calculation can also provide better band gaps and magnetic moments for the systems including transition metals than the PBE calculation;[45−50] therefore, we have considered PBE+$U$ methods for the TM−phosphorene systems.

## RESULTS AND DISCUSSION

**Mono- and Divacancy Defects.** We created vacancy defects by removing P atoms from the upper and/or lower half layers in pristine phosphorene (Figure 1a). In particular, we considered monovacancy (MV) (Figure 1b) and two different types of divacancies: planar divacancy ($DV_P$) (Figure 1c) and staggered divacancy ($DV_S$) (Figure 1d). In a $DV_P$, two neighboring P atoms (i.e., a P dimer) are removed from the same half layer, while in a $DV_S$, two neighboring P atoms are removed from adjacent upper and lower half layers (Figure 1a).

The vacancy formation energy ($\Delta E_{vac}$) is defined as

$$\Delta E_{vac} = (E_{ph+v} + nE_P) - E_{ph}$$

where $E_{ph+v}$ and $E_{ph}$ are the total energies of phosphorene with and without vacancies, respectively. $E_P$ is the per-atom energy of bulk black phosphorus, and $n$ denotes the number of missing atoms with a vacancy in the phosphorene.

The $\Delta E_{vac}$ depends critically on the strengths of bond breaking and formation during the vacancy creation. Our calculations show that $\Delta E_{vac}$ for an MV is 1.71 eV. Formation of the MV defect in the phosphorene initially creates three dangling bonds around the MV, but Jahn−Teller distortion saturates two of the three, which are at different half-layers, by bond formation between two (Figure 1b). The system then leads to a magnetic moment of 1.0 $\mu_B$ at the remaining dangling bond (Figure 1b and Table 1).

Moreover, the MV leads to an in-gap down-spin state approximately 0.3 eV above the VBM. The main contribution to the in-gap state comes from the $3p_x$ and $3p_y$ states of the P atom with a dangling bond. The existence and position of the in-gap state are quite robust under the change in concentration of the MV defect; the energy positions of in-gap states in three different supercells are the same. Additionally, there is no qualitative difference between our results for MV at both PBE and HSE levels, except that the band gap has increased and the in-gap states are close to the center of the band gap of MV−phosphorene at the HSE level (Figure S2) or the energy distance from CBM to the in-gap state is almost the same, while only that from VBM to the in-gap state is changed. The spin density of the phosphorene sheet with an MV is mainly concentrated at the P atoms with broken bonds (Figure 1b). We have found from our ABMD test that the MV structure does not change and does not move to the other half-layer or jump to the other site, which proves the structural stability of our MV structure (Figure S3).

For the $DV_P$−phosphorene, the $\Delta E_{vac}$ is 1.57 eV. After structural relaxation, P atoms around $DV_P$ form four hexagons, two pentagons, and one octagon—a structure that is similar to the 5−8−5 defect in graphene. The rearrangement of atoms and saturation of all dangling bonds lowers the $\Delta E_{vac}$ and, surprisingly, leading to $\Delta E_{vac}$ for the $DV_P$−phosphorene that is ∼0.14 eV lower than that of the MV−phosphorene. This result indicates that knocking out a phosphorus dimer ($DV_P$) compared with a single P atom from pristine phosphorene is energetically easier. We cross checked formation energies and defective geometry using LDA,[53] but the optimized structure of


DOI: 10.1021/jp5110938
J. Phys. Chem. C 2015, 119, 6530−6538

MV is qualitatively different from HSE-relaxed geometry, while PBE-relaxed MV structure agrees very well (Figure S8) with the HSE-relaxed geometry. Thus, we use PBE-relaxed structures throughout this paper. The $DV_S$ creates dangling bonds at four P atoms, two in each half layer. After relaxations, P atoms (in each layer) with dangling bonds come slightly close to each other (shown by the dotted line in Figure 1d) and form weak bonds, which lead to 3.14 eV of high $\Delta E_{vac}$. The methodology used to describe the dangling bond is explained in detail in the Supporting Information (Figure S9). Our DFT calculations indicate that both $DV_P$− and $DV_S$−phosphorene are nonmagnetic; however, there are in-gap states close to the VBM in the DVs−phosphorene, whereas the $DV_P$−phosphorene has no in-gap state (Figure 1f).

**Adatom on Pristine Phosphorene.** In addition to vacancies, we also investigated the effects of adsorbed adatoms on the electronic structure of phosphorene. We considered an omnipresent nonmagnetic adatom $X$ ($X$ = C, N, O) and a magnetic adatom ($X$ = Fe, Co, Ni) on phosphorene. We considered various adsorption sites, atom top, in-plane bridge and hollow (shown as 3, 4 in Figure 1c), on phosphorene (Figure 1a). The optimized structures for each adatom are shown in Figure S4. The C adatom displaces a P atom away from its original site and occupies the hollow site. N and O adatoms also prefer the hollow site. However, the C adatom is within the phosphorene plane, while the N and O adatoms are out of the plane in which C, N, and O adatoms are bonded with three, two, and one P atom(s), respectively. Additionally, the TM adatoms stay over the hollow site. Table S1 shows the shortest and longest distances between the TM adatom and the surrounding P atoms.

Figure 2a shows the total and projected DOSs of C-, N-, and O-adsorbed phosphorene. For C-adsorbed phosphorene, in-gap states appear in both up- and down-spin states approximately 0.5 eV above the highest occupied state, which is a mixture of the $2p_z$ of the C adatom and $3p_x$ of the P atoms around the C-adatom. For N-adsorbed phosphorene, a very narrow in-gap up-spin state appears approximately 0.4 eV above the highest occupied state, which is the 3s, $3p_x$, and $3p_y$ states of the P atom bonded to the adatom, and the down-spin state is directly on the VBM. Interestingly, for the N-adsorbed phosphorene, the in-gap state and the state at the up-spin VBM are very narrow, indicating a strong confinement of the state. The O-adatom does not induce any in-gap states or spin-polarized states, although it increases the band gap by 0.12 eV. This clearly shows that O-adsorbed phosphorene hardly changes the magnetic properties of phosphorene. The HSE calculation also predicts the presence of the in-gap states for C-/N-adsorbed pristine phosphorene (Figure 2b), although their positions within the forbidden gap of pristine phosphorene are different from those obtained from the PBE calculations.

We find that the TM adatoms stay over the hollow region, making three nonequivalent bonds with three P atoms (Table S1 and Figure S4d). P atoms around the TM adatoms approach each other, distorting the sheet mainly in the planar direction. For Fe- or Co-adsorbed phosphorene (Figure 2a), the up/down-spin states primarily coming from the 3d orbitals of the TM become the highest occupied states and are well localized, similar to the case of N-adsorbed phosphorene. In particular, Co 3d states appear as in-gap states in down-spin states for Co-adsorbed phosphorene. However, for Ni-adsorbed phosphorene, the Ni 3d states contribute to both the VBM and CBM, showing that no in-gap state or dispersionless state appears.

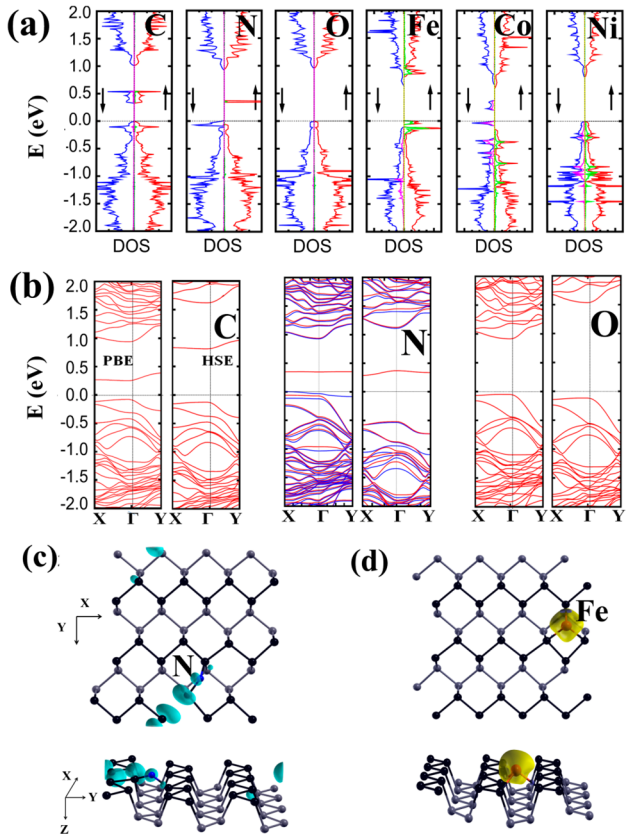


**Figure 2.** Adatom adsorption on pristine phosphorene. (a) DOS, (b) band structures, and (c, d) geometric structures and spin density. (b) Band structures from PBE (left) and HSE (right) calculations were compared. In (a), red and blue lines indicate spin-up and -down of total DOS, while green and magenta lines indicate PDOS of C/N/O 2p and TM 3d, respectively. (b) Spin-up and -down bands for C and O are the same, while they are different for N. The highest occupied state was set to zero.

After Fe, Co, and Ni adsorption, the band gap decreases by approximately 0.2, 0.6, and 0.1 eV, respectively.

**Adatoms at Defected Phosphorene with the MV or DV.** For 2D systems such as graphene[54] or *h*-BN,[55] vacancy defects provide an effective way to enhance the stability of adsorbed adatoms. Because of structural distortions and unsaturated bonds, a vacancy can increase the chemical activities of the 2D systems toward adatom adsorption. $DV_S$−phosphorene was not considered in this study because it is less favorable than the $DV_P$−phosphorene ("P" is omitted henceforth). The adsorption energy ($E_{ads}$) and formation energy ($\Delta E$) values for adatoms adsorbed on the MV− and DV−phosphorene are presented in Table 1. Indeed, the more negative $E_{ads}$ and $\Delta E$ values of adatoms from the adatom-adsorbed MV−phosphorene system indicate increased stability compared to pristine phosphorene. We find that all of the adatoms form stable chemical bonds with unsaturated P atoms, and such a structure can be considered as a "*substitutional impurity*" or "*substitutional doping*", as shown in Figure S4e. The bond distances between the P and TM atoms are slightly shorter (approximately 5%) than the sum of their covalent radii, indicating that the adatoms are slightly displaced toward the inner side of the half layer, which leads to the negative values of elevation above the phosphorene.



DOI: 10.1021/jp5110938
J. Phys. Chem. C 2015, 119, 6530−6538

The DOS of adatom-adsorbed MV−phosphorene is shown in Figure 3a. The $2p_z$ state of the C adatom interacts with the

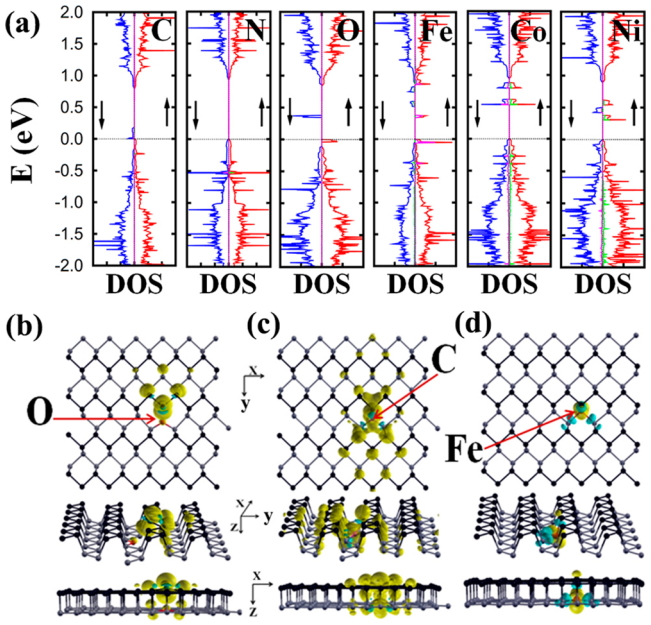


**Figure 3.** Adatom adsorption on MV−phosphorene. (a) DOS and (b−d) spin density. Red and blue lines in DOS plots indicate spin-up and -down of total DOS, while green and magenta lines indicate PDOS of the 2p of C/N/O and 3d of TM adatoms, respectively. The highest occupied state was set to zero.

$3p_z$ and $3p_y$ states of the P atom (with a dangling bond), and defect states with a long tail in the armchair direction are induced. Because of this long tail, defect states for different C atoms can interact with each other even in low concentrations, which is evidenced by the observation that the magnetic moment from a C adatom disappears at a 4 × 3 supercell (2% concentration), while it is preserved for all other adatoms and defects at the same size of supercells. Because the N atom has the same outer shell structure as the P atom for N-adsorbed MV−phosphorene, the electronic structure is very similar to pristine phosphorene. O-adsorbed MV−phosphorene has in-gap down-spin states located 0.35 eV above the highest occupied defect state, which is a mixture of the $3p_z$, $3p_y$, and 3s states of the P atom (in the other half layer) bonded to the O atom. This characteristic is similar to the case of the N-adsorbed pristine phosphorene with interchanged up-spin and down-spin states.

As the concentration changes from 0.5% to 2%, adsorption energies decrease very slightly within a range of 0.02−0.2 eV (Table S3), which indicates that up to 2% of the defects and adatoms can be considered isolated. Electronic structures and magnetic moments are also qualitatively same for all the concentrations, except for the C-adsorbed MV−phosphorene described in the previous paragraph.[56]

The strong interaction between MV−phosphorene and TM adatoms substantially modifies the electronic structure of defective phosphorene: conduction band states come down in energy, and the DOS spreads over a large region within the band gap. Compared to the bare MV−phosphorene, the band gap is reduced to 0.45 eV in Fe-adsorbed phosphorene. TM 3d states appear as in-gap states in the up-spin channel of Fe-adsorbed phosphorene and for both up- and down-spin channels in Co-/Ni-adsorbed MV−phosphorene (Figure 3a). We also find that the induced magnetic moment and position of in-gap states remain unchanged even though the supercell size is increased.

For the adatom adsorption on DV−phosphorene, we considered four different positions (Figure 1c). The minimum-energy structures of adatom-adsorbed DV−phosphorene are shown in Figure S4f−h. While the C adatom prefers to adsorb over site "2" in Figure 1c, N/Fe/Co/Ni adatoms prefer site "1" and O adatoms stay over the top of a P atom (Figure S4h). DV-phosphorene has no dangling bond, and due to the large hollow area at the DV, adatoms are less strongly bonded to phosphorene compared with MV−phosphorene, which leads to $E_{ads}$ and $\Delta E$ values similar to those of pristine phosphorene. However, it was energetically favorable for O adatoms to adsorb over the P atom forming a 5-atom ring near DV. Weak bonding of the adatom with the P atoms around the DV produces longer bond lengths between them and a higher elevation of the adatom over the DV−phosphorene (Table S1). With decreasing concentrations of defects due to the relaxation of DV, the adatoms (except C and O) move closer to DV and eventually go inside the hollow region at DV at a 0.5% concentration of the defect. For Fe/Ni adatoms, the resulting structures become energetically favorable for 1% and 0.5% concentrations of the defects (Table 1 and Table S4). Although adsorption energies decrease considerably for all of the adatoms when the concentration of defects is reduced, the magnetic moment of the adatom-adsorbed DV−phosphorene remained same.

The DOS of adatom-adsorbed DV−phosphorene is similar to that of adatom-adsorbed pristine phosphorene (Figure 4a) in terms of the in-gap states or spin-polarized states that appear. However, for N- or Fe-adsorbed DV−phosphorene, additional in-gap states are produced due to their interaction with the N-2p and Fe-3d states.

Whether phosphorene adsorbed with a nonmetallic adatom has a magnetic moment is determined by a simple rule: if the

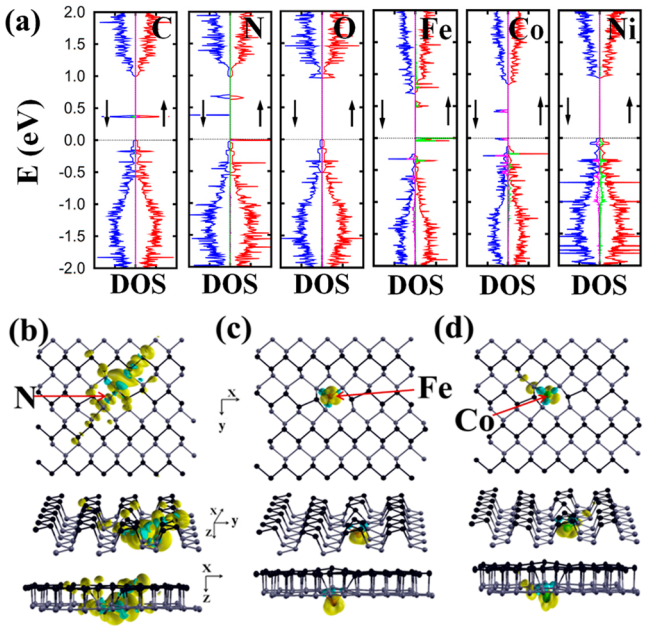


**Figure 4.** Adatom adsorption on DV-phosphorene. (a) DOS and (b−d) spin density for DV−phosphorene with adsorbed adatom.



DOI: 10.1021/jp5110938
J. Phys. Chem. C 2015, 119, 6530−6538

adatom-adsorbed phosphorene (pristine/MV/DV) system has an odd number of electrons (e.g., N-adsorbed pristine (Figure 2c), O-/C-adsorbed MV (Figures 3b,c), and N-adsorbed DV (Figure 4b)), the system has a magnetic moment of 1.0 $\mu_B$; otherwise, the system is nonmagnetic. To support this rule, we additionally investigated the magnetic properties of pristine phosphorene when two N adatoms are adsorbed. Because the system has an even number of electrons, our simple rule predicts that it would show a nonmagnetic property. Our DFT calculation (Figure S5) reveals that the system has, indeed, a nonmagnetic property.

As both N and O atoms are smaller but more electronegative than a P atom, bonding of P with N or O stretches the nearby P−P bond, leaving one P atom with a broken bond. Figures 2c and 3b show the spin density of N-adsorbed pristine and O-adsorbed MV-phosphorene. While the magnetic moment mainly comes from the P atoms with broken bonds, a small moment also appears on the adatoms and nearby P atoms.

Our calculated values for the magnetic moments of Fe-, Co-, and Ni-adsorbed phosphorene are 2.0, 1.0, and 0.0 $\mu_B$, respectively.[57] MV−phosphorene has an odd number of electrons and has a magnetic moment of 1.0 $\mu_B$; therefore, after adsorption of TM adatoms, the magnetic moment further decreases to 1.0 $\mu_B$. In contrast, DV−phosphorene has an even number of electrons, giving it the same value of an induced magnetic moment as pristine phosphorene. For TM-adsorbed phosphorene systems, the magnetic moment is mainly localized on the TM adatom (Figures 2d, 3d, and 4c,d).

We also considered $O_2$ adsorption on pristine and MV− and DV−phosphorene. The $O_2$ molecule is spontaneously dissociated into two O atoms over pristine/defected phosphorene, which is similar to previous reports.[58,59] In the present study, we concentrate on the $O_2$ adsorption over the defective phosphorene. After the dissociation, the O atoms bind to P atoms close to vacancy that are not the nearest neighbors and lie out of the phosphorene plane (Figure 5b,c). The $\Delta E$ for the chemisorbed (dissociated) $O_2$ molecule is more stable by 4.5 eV relative to an isolated $O_2$ molecule, which is almost 2 times higher than the $\Delta E$ of an O atom on pristine phosphorene. We also considered adsorption of a second O adatom when one O adatom is already adsorbed on the MV− or DV−phosphorene. Our calculation shows that both of the O atoms prefer binding with two different P atoms in the phosphorene rather than forming an $O_2$ molecule, which is consistent with the spontaneous dissociation reaction of the $O_2$ molecule on vacancies of phosphorene.

It is interesting that the electronic structures of defective phosphorene with an MV or DV are maintained even after $O_2$ adsorption, as shown in Figure 5e,f. Their magnetic moments also remain the same before and after $O_2$ adsorption. In other words, $O_2$-adsorbed MV−phosphorene has a magnetic moment of 1.0 $\mu_B$, where the magnetic moment is mainly located on P atoms near the MV of phosphorene (Figure 5b), similar to the case of MV−phosphorene without adatoms. These results indicate that the defective phosphorene with an MV can be easily oxidized and stabilized, but its electronic and magnetic properties are unchanged after the $O_2$ adsorption. Therefore, a metal-free magnetic material can be developed by the oxidation of defective phosphorene.

As several structures of phosphorene with vacancies or adatoms have spin-polarized states in the gap or near the valence band maximum, it is possible to tune the magnetic moment by controlling the Fermi level or by charging the

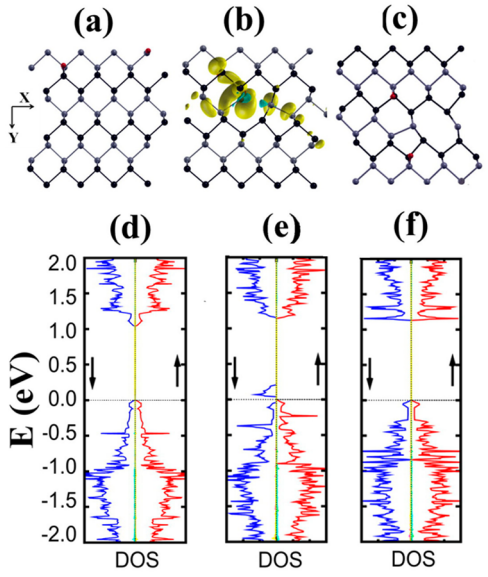


**Figure 5.** $O_2$ adsorption on (a, d) pristine, (b, e) MV−, and (c, f) DV−phosphorene. Red and blue lines indicate spin-up and spin-down of total DOS, while green, cyan, magenta, and yellow represent the PDOS of two oxygen atoms. A spin density plot for the MV−phosphorene after $O_2$ adsorption is shown in (b). The highest occupied state was set to zero.

phosphorene. In general, this can be achieved by, for example, a vertically applied electric field in back gate structure, similar to the recent suggestion by Huang et al.,[55] or by using appropriate supporting substrate that can induce the desired electron transfer from/to phosphorene. In this study, we mimic general situation by changing total number of electrons in the system. N-adsorbed pristine/DV−phosphorene have fully polarized states located just below and above the Fermi level. Depending on the electron filling configurations, it can be magnetic or nonmagnetic, as shown in Table 2. Similar behavior is also

**Table 2. Magnetic Moment of Adatom-Adsorbed Phosphorene with an Extra Electron (−1*e*: Removing One Electron; +1*e*: Adding One Electron)[a]**

| | magnetic moment ($\mu_B$) | | |
|---|---|---|---|
| adatom (phosphorene) | −1*e* | 0 | +1*e* |
| MV | 0.0 | 1.0 | 0.0 |
| N (pristine) | 0.0 | 1.0 | 0.0 |
| Fe (pristine) | 3.0 | 2.0 | 3.0 |
| Co (pristine) | 2.0 | 1.0 | 0.0 |
| O (MV) | 0.0 | 1.0 | 0.0 |
| C (MV) | 0.0 | 1.0 | 0.0 |
| Fe (MV) | 2.0 (3.1) | 1.0 (1.0) | 0.0 (0.0) |
| N (DV) | 0.0 | 1.0 | 0.0 |
| Co (DV) | 2.0 | 1.0 | 0.0 |

[a]For an Fe-adsorbed MV−phosphorene system, magnetic moments from PBE+*U* calculations ($U_{3d}$ = 6 eV) are given in the parentheses.

found in the O-adsorbed MV−phosphorene (Figure 6a). In the TM-adsorbed structures (Figure 6b), both the on/off transition of the magnetic moment and its strength can be tuned. Co-adsorbed pristine phosphorene has a magnetic moment of 1.0 $\mu_B$, and its spin-minority states are at just above and below the Fermi level. Consequently, the magnetic moment can be tuned


DOI: 10.1021/jp5110938
J. Phys. Chem. C 2015, 119, 6530−6538

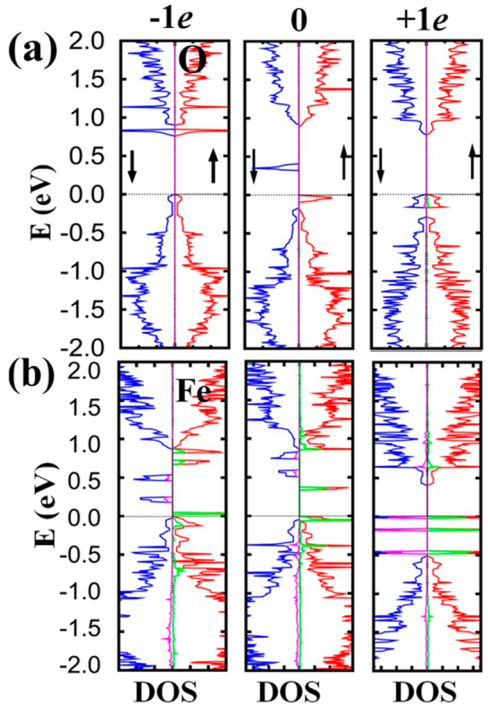


**Figure 6.** Change in magnetic moments of (a) O- and (b) Fe-adsorbed MV−phosphorene with different filling configurations. (−1*e*: removing an electron; +1*e*: adding an electron) The magnetic moment for an O adatom can be switched ON/OFF, while it can be varied from 2.0 to 1.0 and then to 0.0 $\mu_B$ (left to right) for an Fe adatom.

to 2.0 $\mu_B$ by lowering the Fermi level and to 0.0 $\mu_B$ by elevating the Fermi level.

For Fe-adatom MV−phosphorene, we also performed PBE+*U* calculations to investigate the effects of electron correlation on the electronic and magnetic properties of the system including a transition metal element, where *U* = 2, 4, and 6 eV were considered. Using the 6 × 4 supercell for phosphorene,[60] we found that an induced magnetic moment of the system is 1.0 $\mu_B$ irrespective of the *U* values and that spins of Fe and P atoms are antiparallel to each other, as shown in Figure S6. In Table 2, the PBE+*U* calculations also show that the addition of an electron makes the system a nonmagnetic semiconductor, while the removal of an electron makes the system a magnetic metal. Thus, we can confirm that the PBE and PBE+*U* calculations provide similar magnetic properties for the phosphorene system including a TM adatom.

## CONCLUSIONS

In conclusion, we have systematically studied the effects of vacancy defects and the adsorption of nonmetallic C/N/O and Fe/Co/Ni TMs on the electronic and magnetic properties of phosphorene using DFT calculations. Our calculations show that the vacancies and adatoms can tune the electronic and magnetic properties of phosphorene. Because as-synthesized phosphorene can include defects or impurities, we can readily tune the electronic and magnetic properties of phosphorene by means of these defects or impurities. Moreover, we find that a metal-free magnetic material that exhibits good stability can be developed by oxidation of the defective phosphorene. Our results provide a novel pathway for achieving metal-free and tunable magnetism as well as a tunable band gap for various possible applications of phosphorene.

## ASSOCIATED CONTENT

### Supporting Information

Table S1 shows the geometrical parameters for a 2% concentration of adatoms; in Tables S2, S3, and S4, adsorption energies and formation energies at different concentrations of adatoms adsorbed over pristine, MV−, and DV−phosphorene, respectively, are presented; various sizes of supercells taken in this study, comparison of electronic structures of pristine, bare, and C-adsorbed MV−phosphorene obtained from PBE and HSE06 methods, time evolution of MV−phosphorene, optimized structures of defected phosphorene with adatoms (C, N, O, Fe, Co, and Ni), magnetic coupling between two N-adsorbed pristine phosphorene as a function of distance between them and electronic structure and spin-density plots for Fe-adsorbed MV−phosphorene with included correlation effects are displayed in Figures S1, S2, S3, S4, S5, and S6, respectively; DOS and PDOS of different adatom adsorbed pristine/defective phosphorene for 2% concentration of defect and internal structure of MV at HSE, PBE, and LDA level and of $DV_P$ and $DV_S$ at PBE level are shown in Figures S7 and S8, respectively; a discussion regarding the convergence of stress tensor with system size is provided. Figure S9 shows our methodology to define broken bonds. This material is available free of charge via the Internet at http://pubs.acs.org.

## AUTHOR INFORMATION

### Corresponding Authors

*(S.S.H.) E-mail sangsoo@kist.re.kr, Tel +82-2-958-5441.
*(S.K.) E-mail sckim@kist.re.kr, Tel +82-2-958-5491.

### Notes

The authors declare no competing financial interest.

## ACKNOWLEDGMENTS

We acknowledge the financial support of the Korea Institute of Science and Technology Institutional projects (Grant No. 2E25372) and the Industrial Strategic Technology Development Program (Grant No. 10041589) funded by the Ministry of Trade, Industry, and Energy (MOTIE) of Korea. We are also thankful for the use of the IMR supercomputers facility at Tohoku University, Japan.

## REFERENCES

(1) Liu, H.; Neal, A. T.; Zhu, Z.; Tománek, D.; Ye, P. D. Phosphorene: An Unexplored 2D Semiconductor with a High Hole Mobility. *ACS Nano* **2014**, *8*, 4033−4041.
(2) Li, L.; Yu, Y.; Ye, G. J.; Ge, Q.; Ou, X.; Wu, H.; Feng, D.; Chen, X. H.; Zhang, Y. Black Phosphorus Field-Effect Transistors. *Nat. Nanotechnol.* **2014**, *9*, 372−377.
(3) Xia, F.; Wang, H.; Jia, Y. Rediscovering Black Phosphorus: A Unique Anisotropic 2D Material for Optoelectronics and Electronics. *Nat. Commun.* **2014**, *5*, 4458(1)−4458(6).
(4) Koenig, S. P.; Doganov, R. A.; Schmidt, H.; Castro Neto, A. H.; Oezyilmaz, B. Electric Field Effect in Ultrathin Black Phosphorus. *Appl. Phys. Lett.* **2014**, *104*, 103106−4.
(5) Deng, Y.; Luo, Z.; Conrad, N. J.; Liu, H.; Gong, Y.; Najmaei, S.; Ajayan, P. M.; Lou, J.; Xu, X.; Ye, P. D. Black Phosphorous-Monolayer $MoS_2$ van der Waals Heterojunction p-n Diode. *ACS Nano* **2014**, *8*, 8292−8299.
(6) Du, Y.; Ouyang, C.; Shi, S.; Lei, M. *Ab-initio* Studies on Atomic and Electronic Structures of Black Phosphorus. *J. Appl. Phys.* **2010**, *107*, 093718−4.
(7) Tran, V.; Soklaski, R.; Liang, Y.; Yang, L. Layer-Controlled Band Gap Anisotropic Excitons in Few-Layer Black Phosphorous. *Phys. Rev. B* **2014**, *89*, 235319−6.


DOI: 10.1021/jp5110938
*J. Phys. Chem. C* 2015, 119, 6530−6538

(8) Qiao, J.; Kong, X.; Hu, Z.-X.; Yang, F.; Ji, W. High-Mobility Transport Anisotropy and Linear Dichroism in Few Layer Black Phosphorus. *Nat. Commun.* **2014**, *5*, 4475(1)−4475(7).
(9) Fei, R.; Yang, L. Strain-Engineering Anisotropic Electrical Conductance of Phosphorene and Few-Layer Black Phosphorous. *Nano Lett.* **2014**, *14*, 2884−2889.
(10) Ong, Z.-Y.; Cai, Y.; Zhang, Y.-W. Strong Thermal Transport Anisotropy and Strain Modulation in Single-Layer Phosphorene. *J. Phys. Chem. C* **2014**, *118*, 25272−25277.
(11) Rodin, A. S.; Carvalho, A.; Castro Neto, A. H. Strain-Induced Gap Modification in Black Phosphorus. *Phys. Rev. Lett.* **2014**, *112*, 176801(1)−176801(5).
(12) Peng, X.; Copple, A.; Wei, Q. Strain Engineered Direct-Indirect Band Gap Transition and its Mechanism in 2D Phosphorene. *Phys. Rev. B* **2014**, *90*, 085402(1)−085402(10).
(13) Guo, H.; Lu, N.; Dai, J.; Wu, X.; Zeng, X. C. Phosphorene Nanoribbons, Phosphorus Nanotubes and van der Waals Multilayers. *J. Phys. Chem. C* **2014**, *118*, 14051−14059.
(14) Maity, A.; Singh, A.; Sen, P. Peierls Transition and Edge Reconstruction in Phosphorene Nanoribbons. 2014, arXiv: 1404.2469. arXiv preprint; http://arxiv.org/abs/1404.2469.
(15) Tran, V.; Yang, L. Scaling Laws of the Band Gap and Optical Response of Phosphorene Nanoribbons. *Phys. Rev. B* **2014**, *89*, 245407(1)−245407(5).
(16) Carvalho, A.; Rodin, A. S.; Castro Neto, A. H. Phosphorene Nanoribbons. *Eur. Phys. Lett.* **2014**, *108*, 47005(1)−47005(6).
(17) Dai, J.; Zeng, X. C. Bilayer Phosphorene: Effect of Stacking Order on Band Gap and Its Potential Applications in Thin-Film Solar Cells. *J. Phys. Chem. Lett.* **2014**, *5*, 1289−1293.
(18) Sa, B.; Li, Y.-L.; Qi, J.; Ahuja, R.; Sun, Z. Strain Engineering for Phosphorene: The Potential Application as a Photocatalyst. *J. Phys. Chem. C* **2014**, *118*, 26560−26568.
(19) Sun, L. Q.; Li, M.-J.; Sun, K.; Yu, S.-H.; Wang, R.-S.; Xie, H.-M. Electrochemical Activity of Black Phosphorus as an Anode Material for Lithium-Ion Batteries. *J. Phys. Chem. C* **2012**, *116*, 14772−14779.
(20) Kulish, V. V.; Malyi, O. I.; Persson, C.; Wu, P. Evaluation of Phosphorene as Anode Material for Na-ion Batteries from First Principles. 2015, arXiv: 1501.02425. arXiv preprint; http://arxiv.org/abs/1501.02425.
(21) Zhang, C. D.; Lian, J. C.; Yi, W.; Jiang, Y. H.; Liu, L. W.; Hu, H.; Xiao, W. D.; Du, S. X.; Sun, L. L.; Gao, H. J. Surface Structures of Black Phosphorous Investigated with Scanning Tunneling Microscopy. *J. Phys. Chem. C* **2009**, *113*, 18823−18826.
(22) Wang, L.; Wang, Y.; Chen, X.; Zhu, W.; Zhu, C.; Wu, Z.; Han, Y.; Zhang, M.; Li, W.; He, Y.; et al. Negative Quantum Capacitance Induced by Midgap States in Single-layer Graphene. *Sci. Rep.* **2013**, *3*, 2041(1)−2041(5).
(23) Ghorbani-Asl, M.; Enyashin, A. N.; Kuc, A.; Seifert, G.; Heine, T. Defect-Induced Conductivity Anisotropy in $MoS_2$ Monolayers. *Phys. Rev. B* **2013**, *88*, 245440(1)−245440(7).
(24) Castellanos-Gomez, A.; Vicarelli, L.; Prada, E.; Island, J. O.; Narshimha-Acharya, K. L.; Blanter, S. I.; Groenendijk, D. J.; Buscema, M.; Steele, G. A.; Alvarez, J. V.; et al. Isolation and Characterization of Few-Layer Black Phosphorous. *2D Mater.* **2014**, *1*, 025001(1)−025001(19).
(25) Favron, A.; Gaufrès, E.; Fossard, F.; Lèvesque, L. P.; Phaneuf-L'Heureux, A.-L.; Tang, N. Y-W.; Loiseau, A.; Leonelli, R.; Sèbastien, F.; Martel, R. Exfoliating Pristine Black Phosphorus Down to the Monolayer: Photo-Oxidation and Quantum Confinement. 2014, arXiv: 1408.0345. arXiv preprint; http://arxiv.org/abs/1408.0345.
(26) Bridgman, P. W. Two New Modifications of Phosphorus. *J. Am. Chem. Soc.* **1914**, *36*, 1344−1363.
(27) Kresse, G.; Furthmüller, J. Efficient Iterative Schemes for *Ab-Initio* Total-Energy Calculations Using a Plane-Wave Basis Set. *Phys. Rev. B* **1996**, *54*, 11169−11186.
(28) Kresse, G.; Furthmüller, J. Efficiency of *Ab-Initio* Total Energy Calculations for Metals and Semiconductors Using a Plane-Wave Basis Set. *Comput. Mater. Sci.* **1996**, *6*, 15−50.
(29) Perdew, J. P.; Burke, K.; Ernzerhof, M. Generalized Gradient Approximation Made Simple. *Phys. Rev. Lett.* **1996**, *77*, 3865−3868.
(30) Blöchl, P. E. Projector Augmented-Wave Method. *Phys. Rev. B* **1994**, *50*, 17953−17979.
(31) Grimme, S. Semiempirical GGA-Type Density Functional Constructed with a Long Range Dispersion Correction. *J. Comput. Chem.* **2006**, *27*, 1787−1799.
(32) Nosé, S. A Unified Formulation of the Constant Temperature Molecular Dynamics Methods. *J. Chem. Phys.* **1984**, *81*, 511−519.
(33) Nosé, S. Constant Temperature Molecular Dynamics Methods. *Prog. Theor. Phys. Suppl.* **1991**, *103*, 1−46.
(34) Bylander, D. M.; Kleinman, L. Energy Fluctuations Induced by the Nosé Thermostat. *Phys. Rev. B* **1992**, *46*, 13756−13761.
(35) Monkhorst, H. J.; Pack, J. D. Special Points for Brillouin-Zone Integrations. *Phys. Rev. B* **1976**, *13*, 5188−5192.
(36) Brown, A.; Rundqvist, S. Refinement of the Crystal Structure of Black Phosphorous. *Acta Crystallogr.* **1965**, *19*, 684−685.
(37) Cartz, L.; Srinivasa, S. R.; Riedner, R. J.; Jorgensen, J. D.; Worlton, T. G. Effect of Pressure on Bonding in Black Phosphorus. *J. Chem. Phys.* **1979**, *71*, 1718−1721.
(38) Heyd, J.; Scuseria, G. E.; Ernzerhof, M. Hybrid Functionals Based on a Screened Coulomb Potential. *J. Chem. Phys.* **2003**, *118*, 8207−8215.
(39) Li, Y.; Yang, S.; Li, J. Modulation of the Electronic Properties of Ultrathin Black Phosphorous by Strain and Electric Field. *J. Phys. Chem. C* **2014**, *118*, 23970−23976.
(40) Keyes, R. W. The Electrical Properties of Black Phosphorus. *Phys. Rev. B* **1953**, *92*, 580−584.
(41) Warschauer, D. Electrical and Optical Properties of Crystalline Black Phosphorus. *J. Appl. Phys.* **1963**, *34*, 1853−1860.
(42) Dudarev, S. L.; Botton, G. A.; Savrasov, S. Y.; Humphreys, C. J.; Sutton, A. P. Electron-Energy-Loss Spectra and the Structural Stability of Nickel Oxide: An LSDA+*U* Study. *Phys. Rev. B* **1998**, *57*, 1505−1509.
(43) Anisimov, V. I.; Gunnarsson, O. Density-Functional Calculation of Effective Coulomb Interactions in Metals. *Phys. Rev. B* **1991**, *43*, 7570−7574.
(44) Loschen, C.; Carrasco, J.; Neyman, K. M.; Illas, F. First-Principles LDA+*U* and GGA+*U* Study of Cerium Oxides: Dependence on the Effective *U* Parameter. *Phys. Rev. B* **2007**, *75*, 035115(1)−035115(8).
(45) Nolan, M.; Watson, G. W. Hole Localization in Al Doped Silica: A DFT+*U* Description. *J. Chem. Phys.* **2006**, *125*, 144701(1)−144701(6).
(46) Dompablo, M. E. A.; Morales-Garcia, A.; Travillo, M. DFT+*U* Calculations of Crystal Lattice, Electronic Structure, and Phase Stability under Pressure of $TiO_2$ Polymorphs. *J. Chem. Phys.* **2011**, *135*, 054503−9.
(47) Silva, J. L. F. Da; Ganduglia-Pirovano, M. V.; Sauer, J. Formation of the Cerium Orthovandate $CeVO_4$: DFT+*U* Study. *Phys. Rev. B* **2007**, *76*, 125117(1)−125117(10).
(48) Getsoian, A. B.; Shapovalov, V.; Bell, A. T. DFT+*U* Investigation of Propene Oxidation over Bismuth Molybdate: Active Sites, Reaction Intermediates, and the Role of Bismuth. *J. Phys. Chem. C* **2013**, *117*, 7123−7137.
(49) Schrön, A.; Rödl, C.; Bechstedt, F. Energetic Stability and Magnetic Properties of MnO in the Rocksalt, Wurtzite, and Zinc-Blende Structures: Influence of Exchange and Correlation. *Phys. Rev. B* **2010**, *82*, 165109(1)−165109(12).
(50) Arroyo-de Dompablo, M. E.; Biskup, N.; Gallardo-Amores, J. M.; Moran, E.; Ehrenberg, H.; Amador, U. Gaining Insights into the Energetics of $FePO_4$ Polymorphs. *Chem. Mater.* **2010**, *22*, 994−1001.
(51) Heyd, J.; Peralta, J. E.; Scuseria, G. E.; Martin, R. L. Energy Band Gaps and Lattice Parameters Evaluated with the Heyd-Scuseria-Ernzerhof Screened Hybrid Functional. *J. Chem. Phys.* **2005**, *123*, 174101(1)−174101(8).
(52) Clark, S. J.; Robertson, J.; Lany, S.; Zunger, A. Intrinsic Defects in ZnO Calculated by Screened Exchange and Hybrid Density Functionals. *Phys. Rev. B* **2010**, *81*, 115311(1)−115311(5).


DOI: 10.1021/jp5110938
*J. Phys. Chem. C* 2015, 119, 6530−6538

(53) At the LDA level, obtained values of $\Delta E$ for MV and $DV_P$ are 1.79 and 1.57 eV, respectively.
(54) Krasheninnikov, A. V.; Lehtinen, P. O.; Foster, A. S.; Pyykkö, P.; Nieminen, R. M. Embedding Transition-Metal Atoms in Graphene: Structure, Bonding, and Magnetism. *Phys. Rev. Lett.* **2009**, *102*, 126807(1)−126807(4).
(55) Huang, B.; Xiang, H.; Yu, J.; Wei, S.-H. Effective Control of the Charge and Magnetic States of Transition-Metal Atoms on Single-Layer Boron Nitride. *Phys. Rev. Lett.* **2012**, *108*, 206802(1)−206802(5).
(56) Magnetic moment of C adatom on MV in 4 × 3 supercell in PBE calculation is 0.0 $\mu_B$ because up- and down-spin states at the Fermi level are almost degenerated (≈0.1 eV of splitting), while it is 1 $\mu_B$ in HSE calculation up- and down-spin states split largely (≈0.8 eV of splitting), which indicates that magnetic moment might be survive in 2% of concentration. See Figure S2c in the Supporting Information.
(57) Valencia, H.; Gil, A.; Frapper, G. Trends in the Adsorption of 3d Transition Metal Atoms onto Graphene and Nanotube Surfaces: A DFT Study and Molecular Orbital Analysis. *J. Phys. Chem. C* **2010**, *114*, 14141−14153.
(58) Ziletti, A.; Carvalho, A.; Campbell, D. K.; Coker, D. F.; Castro Neta, A. H. Oxygen Defects in Phosphorene. *Phys. Rev. Lett.* **2014**, *114*, 046801(1)−046801(5).
(59) Wang, G.; Pandey R.; Karna, S. P. Phosphorene Oxide: Stability and Electronic Properties of a Novel 2D Material. 2014, arXiv: 1409.0459. arXiv preprint; http://arxiv.org/abs/1409.0459.
(60) Using the 48-atom supercell for phosphorene, the induced magnetic moment of the Fe-adsorbed MV−phosphorene is 1.0 $\mu_B$ for $U$ = 2 and 4 eV. For $U$ = 6, the magnetic moment of the system becomes 3.0 $\mu_B$. As the $U$ value increases, d-states of a Fe atom move away from Fermi level and p-states of P atoms spread across the Fermi level, which transforms the system from semiconductor to half-metal. It might be a consequence of the finite-size effect.



DOI: 10.1021/jp5110938
*J. Phys. Chem. C* 2015, 119, 6530−6538